First-principles study of the structure and stability of oxygen defects in zinc oxide

Paul Erhart, Andreas Klein, and Karsten Albe
Institut für Materialwissenschaft, Technische Universität Darmstadt, Petersenstr. 23, D-64287 Darmstadt, Germany
(Received 29 March 2005; revised manuscript received 10 June 2005; published 16 August 2005)

A comparative study on the structure and stability of oxygen defects in ZnO is presented. By means of first-principles calculations based on local density functional theory we investigate the oxygen vacancy and different interstitial configurations of oxygen in various charge states. Our results reveal that dumbbell-like structures are thermodynamically the most stable interstitial configurations for neutral and positive charge states due to the formation of a strongly covalent oxygen–oxygen bond. For negative charge states the system prefers a split-interstitial configuration with two oxygen atoms in almost symmetric positions with respect to the associated perfect lattice site. The calculated defect formation energies imply that interstitial oxygen atoms may provide both donor- and acceptor-like defects.

DOI: 10.1103/PhysRevB.72.085213 PACS number(s): 61.72.Bb, 61.72.Ji, 61.82.Fk, 71.55.Gs

I. INTRODUCTION

Zinc oxide is a transparent semiconductor with a direct band gap of 3.4 eV. It can be degenerately doped *n*-type and free electron concentrations in excess of 10^{21} cm^{-3} are achievable.[1] In recent years *p*-type doping has been reported by several groups (see Ref. 2 and references therein). The ambipolar dopability and the high exciton binding energy render ZnO an interesting material for transparent electronics and blue light emitting devices. As a result of self-compensation, however, for large band-gap materials very often only a single conductivity type can be obtained (see, e.g., Refs. 3 and 4). In that case raising the dopant level will not lead to the generation of free carriers but to the generation of compensating defects.

In order to achieve *p*-type conductivity the Fermi level needs to be close to the valence band. Photoelectron spectroscopy reveals that the valence band in ZnO lies about 7 eV below the vacuum level.[5] If we take 4.5 eV as reference for the standard hydrogen electrode on an absolute energy scale,[6] a Fermi level close to the valence band maximum of ZnO corresponds to a redox potential of $\gtrsim 2.5$ eV. Chemically, such large redox potentials can cause the oxidation of oxygen and thus change the formal oxidation state from O^{-II} to O^{-I} or even further to O^0. The oxidation of oxygen in ZnO can be described in Kröger-Vink notation by

$$O_O^\times + \frac{1}{2}O_2 \rightarrow (O_2)_O^\times$$

suggesting that O_2^{2-} ions occupy O^{2-} lattice sites as in zinc peroxide ZnO_2. To the best of our knowledge, the existence of such interstitial structures has not been explicitly discussed in literature, and we are only aware of a study by Lee *et al.*[7] who have investigated a dumbbell configuration in the context of N acceptors in ZnO. Other theoretical studies[8–11] on intrinsic point defects in ZnO only considered highly symmetric octahedral and tetrahedral sites for interstitial oxygen.

In this study, we therefore carried out a comprehensive study[24] of peroxolike interstitials in comparison to high-symmetry configurations and vacancies in charge states between 2+ and 2−. Our results reveal that interstitial oxygen atoms are most stable in dumbbell configurations and may act both as donor- and acceptor-like defects.

II. METHODOLOGY

A. Computational method

Density functional theory (DFT) calculations within the local-density approximation (LDA) in the Teter-Pade parameterization[12] were performed using the plane-wave pseudopotential code ABINIT.[13,14] It relies on an efficient fast Fourier transform algorithm[15] for the conversion of wave functions between real and reciprocal space, on the adaptation to a fixed potential of the band-by-band conjugate gradient method,[16] and on a potential-based conjugate-gradient algorithm for the determination of the self-consistent potential.[17] We used norm-conserving pseudopotentials due to Troullier and Martins[18] which included the 3*d*-electrons of zinc as part of the valence. The plane-wave basis-set cutoff energy was set to 35 Hartree to achieve convergence of total energies better than 0.05 eV. Orthogonal supercells containing 64 atoms were employed and the irreducible Brillouin zone of the supercell was sampled using 16 *k*-points distributed on a shifted Monkhorst-Pack grid. All calculations are performed at the same supercell size. This neglect of volume relaxation constitutes the leading contribution to the intrinsic error in our calculated formation energies which can be estimated to be less than 0.1 eV.

The crystallographic parameters for ideal wurtzite zinc oxide were determined as $a=3.2005$ Å and $c/a=1.6131$ with an internal relaxation of $u=0.3792$. Within the known restrictions of the LDA these numbers compare well with the experimental values of $a=3.2417$ Å, $c/a=1.6003$, and $u=0.3819$. The formation enthalpy of wurtzite zinc oxide was computed as −4.15 eV/f.u. (f.u.=formula unit) in reasonable agreement with previous calculations and the experimental value of −3.56 eV/f.u. The band gap at the Γ-point is 0.81eV, which is considerably below the experimental value of 3.4 eV, but consistent with previous DFT calculations. (If only the special *k*-points of the supercell calculations are

considered, which do not include the Γ-point, the band gap is 0.50 eV larger.) The discrepancy is due to the well-known band-gap error of density functional theory. The consequences of this shortcoming will be addressed below.

We have furthermore treated the ground state structures of pure oxygen and zinc, since their cohesive energies enter the calculation of the formation energy of zinc oxide as well as the defect formation energies [see Eq. (1)]. In the case of zinc the calculated cohesive energy of −1.801 eV/atom shows the expected overbinding if compared to the experimental value of −1.359 eV/atom, while the lattice constants $a=2.582$ Å (2.660 Å) and $c=4.791$ Å (4.863 Å) agree nicely with the experimental numbers (given in brackets). The oxygen dimer has a calculated bond length of 1.241 Å (1.208 Å) and a dimer energy of 5.854 eV (5.166 eV).

B. Formation energies

At zero Kelvin the defect formation energy in a given charge state q is given by[19]

$$\Omega_D = E_D - \frac{1}{2}(n_{\mathrm{Zn}} + n_{\mathrm{O}})\mu_{\mathrm{ZnO}}^{\mathrm{bulk}} - \frac{1}{2}(n_{\mathrm{Zn}} - n_{\mathrm{O}})(\mu_{\mathrm{Zn}}^{\mathrm{bulk}} - \mu_{\mathrm{O}}^{\mathrm{bulk}}) - q(E_{\mathrm{VBM}} + \mu_e) - \frac{1}{2}(n_{\mathrm{Zn}} - n_{\mathrm{O}})\Delta\mu, \quad (1)$$

where E_D is the total energy of the system in the presence of the defect, n_i is the number of atoms of atom type i, and μ_i^{bulk} is the chemical potential of the pure constituent i in its reference state. The valence band maximum (VBM) and the (electro-)chemical potential of the electrons (Fermi energy) are denoted by E_{VBM} and μ_e, respectively. The range within which the chemical potentials can vary is described by the last term in Eq. (1). The quantity $\Delta\mu$ is restricted by the formation enthalpy ΔH_f of wurtzitic zinc oxide[10] according to $|\Delta\mu| \leqslant |\Delta H_f|$; zinc- and oxygen-rich conditions correspond to $\Delta\mu = -\Delta H_f$ and $\Delta\mu = \Delta H_f$, respectively. In the zero temperature limit the chemical potentials of gaseous oxygen, solid zinc, and zinc oxide equal the cohesive energies. In the context of this paper, we have used the calculated values for the corresponding chemical potentials. It should be noted, however, that our principal findings are not affected by this particular choice.

C. Configurations

In order to identify the most stable structure for the oxygen interstitial defect, we have generated a number of initial configurations. The atomic positions were relaxed using conjugated-gradient minimization until the maximum residual force was less than 4 pN (2.5 meV/Å). Charge states between 2− and 2+ were considered. We identified three distinct configurations corresponding to local minima on the total-energy surface. In the following we will distinguish between the octahedral interstitial ($\mathrm{O_{i,oct}}$), the dumbbell configuration ($\mathrm{O_{i,db}}$) and the rotated dumbbell configuration ($\mathrm{O_{i,db\text{-}rot}}$) the particular properties of which are described in detail in Sec. III B.

For consistency, we also dealt with oxygen and zinc vacancies. Since it has been confirmed by previous first-principles studies that the oxygen vacancy is a negative-U center with the $q=+1$ state being unstable, we only considered the neutral and the doubly charged oxygen vacancy. The zinc vacancy was calculated in the charge states 2−, 1−, and 0.

D. Charge analysis

As a means to obtain a simple semiquantitative measure for comparing different charge states we have calculated partial charges for all atoms in the defective cells using the Bader method.[20] For this purpose we employed codes included in the ABINIT package.

The Bader atom-in-molecule (AIM) method identifies extrema and saddle points in the three-dimensional electron density and uses this information to partition space into polyhedra each of which is associated with one atom that is then assigned the charge confined in the polyhedron volume.

Since the assignment of electron charges to atomic sites is not unique, the absolute values for the partial charges obtained by any of these methods have limited quantitative significance. Therefore in the following we only discuss the relative partial charges; they have been obtained by normalizing the partial charges of the atoms in the defective system with the partial charge of an atom of the same type in an ideal cell which carries a total charge equivalent to the total charge of the supercell containing the defect.

III. RESULTS

We have studied in detail three different configurations for the oxygen interstitial as well as the two types of vacancies. In the following, we will first discuss the thermodynamics of these defects and then describe the geometric and electronic properties which render each configuration distinct. Then we combine the various pieces of information to obtain a more general picture of the relation between electronic structure, formation energies, and charge states.

A. Thermodynamics

Formation energies of native point defects calculated for oxygen- and zinc-rich conditions are shown in Fig. 1. The band gap calculated at the Γ-point is shown by the gray-shaded area while the vertical dotted lines indicate the band gap obtained if only the special k-points of the supercell calculations are considered. Calculated values for a zinc-rich environment and p-type conducting conditions ($\mu_e=0$ eV, VBM) are given in Table I together with results of previous calculations.

Under zinc-rich conditions the oxygen vacancy, $\mathrm{V_O}$, is the most stable defect for all Fermi levels. It shows a transition from the double positively charged state, $\mathrm{V_O^{\cdot\cdot}}$, to the neutral configuration, $\mathrm{V_O^{\times}}$, close to the conduction band minimum (CBM). This finding is in line with the result of Zhang *et al.*[4] but in contrast to Lee *et al.*[7] who predicted the neutral state $\mathrm{V_O^{\times}}$ to be the stable configuration even close to the VBM.

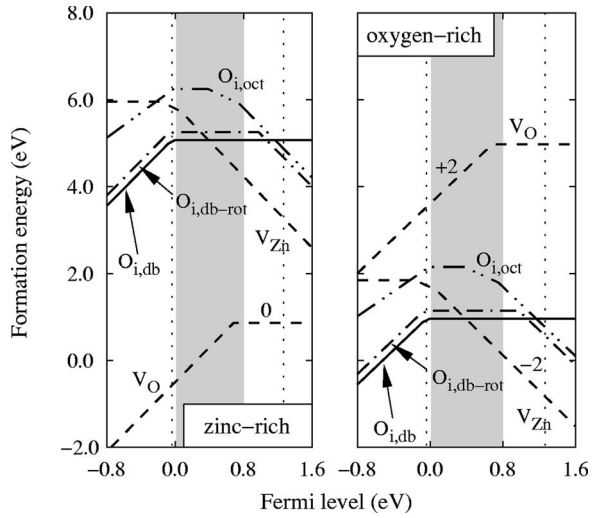

FIG. 1. Variation of the formation energies of several point defects in zinc oxide with the Fermi level under zinc-(left) and oxygen-rich (right) conditions. The numbers in the plot indicate the defect charge state; parallel lines imply equal charge states. The gray-shaded area indicates the band gap calculated at the Γ-point while the vertical dotted lines show the band gap which is obtained if only the special *k*-points of the supercell calculations are considered.

For oxygen-rich conditions, the doubly negatively charged zinc vacancy, V''_{Zn}, is the dominant defect type for Fermi levels in the upper half of the band gap. When the Fermi level lies, however, in the lower half of the band gap our calculations suggest that oxygen interstitials in dumbbell configurations are the dominating point defect type and due to their rather low formation energies should be present in significant amounts. The +2/+1 and +2/0 transition levels for the two dumbbell defects are right at the valence band maximum (Fig. 1). Furthermore, if the band gap is calculated for the special *k*-points (vertical dotted lines in Fig. 1), the 0/−2 transition level for the rotated dumbbell interstitial lies within the band gap just below the conduction band minimum.

In the following sections we will discuss the implications of this finding in more detail by analyzing both electronic structure and geometry. However, before we do so some reasoning is required to which extent our results are affected by the underestimation of the band gap. We resort to a qualitative discussion following the lines of previous works (see Ref. 21 and the Appendix of Ref. 8).

The formation energy corrections for donors in the 2+ charge state are typically large and *negative*; they are smaller for donors in the 1+ and neutral charge states and sometimes even positive. In case of acceptors corrections to the formation energies are usually large and *positive* and of similar magnitude for different charge states. Thus the corrections increase the asymmetry in the formation energies of donor- and acceptor-like defects. These considerations have the following implications on our data presented in Fig. 1: Upon correction of the band gap the formation energies for the 2 + charge states of the oxygen interstitials as well as the oxygen vacancy are expected to be significantly lowered;

TABLE I. Calculated formation energies for oxygen related point defects in bulk zinc oxide for zinc-rich and *p*-type conducting conditions (μ_e=0 eV, VBM); Ref. 8: DFT, LDA, norm-conserving pseudopotentials, Ref. 9: DFT, LDA, ultrasoft pseudopotentials; and Ref. 10: DFT, generalized gradient approximation (GGA), ultrasoft pseudopotentials.

			Ref. 8			
Defect	Charge state	This work	Uncorrected	Corrected	Ref. 9	Ref. 10
V_O	0	0.9	1.5	2.4	0.0	
	+2	−0.5	−0.5	−3.0	−0.3	−0.9
V_{Zn}	0	6.0	5.8	10.6	5.5	⩾5.1
	−1	5.8	5.7	10.1	5.8	5.0
	−2	5.9	5.8	10.1	6.6	5.1
$O_{i,db-rot}$	−2	7.2				(8.2)[a]
	−1	6.6			(7.5)[a]	(⩾7.1)[a]
	0	5.2			(6.5)[a]	(6.0)[a]
	+1	5.3			(6.5)[a]	
	+2	5.4				
$O_{i,oct}$	−2	7.4	7.4[b]	9.7	7.8	7.8
	−1	6.7	6.4	10.4	6.8	6.9
	0	6.2	6.2	12.1	6.4	6.4
	+1	6.3			6.4	
	+2	6.3				
$O_{i,db}$	−2	9.7				
	−1	7.4				
	0	5.1				
	+1	5.1				
	+2	5.2				

[a]References 9 and 10 report formation energies for a "tetrahedral interstitial" configuration but no details on the geometry of the relaxed configuration are given.

[b]The geometry of the oxygen interstitial for which the formation energies are given is not specified in Ref. 8.

whether the formation energy of the 1+ states are lowered or raised cannot be predicted based on our data. On the other hand the formation energies for the neutral and negatively charged defects will rise. If the Fermi level is at the VBM, the formation energies for the various oxygen interstitials display only small differences as the charge state changes from 0 to 2+. Based on the foregoing considerations we therefore expect the presence of a 2+/0 transition level for the oxygen interstitial in the band gap near the VBM. This implies that the oxygen interstitial would effectively act as a donor, since it occurs in a positive charge state. In general, the changes which are expected for the formation energies upon band-gap correction support and emphasize the importance of oxygen interstitials under oxygen-rich conditions.

B. Geometry and electronic structure

1. Vacancies

The oxygen vacancy is the most important intrinsic defect in zinc oxide under zinc-rich conditions. It displays a transi-

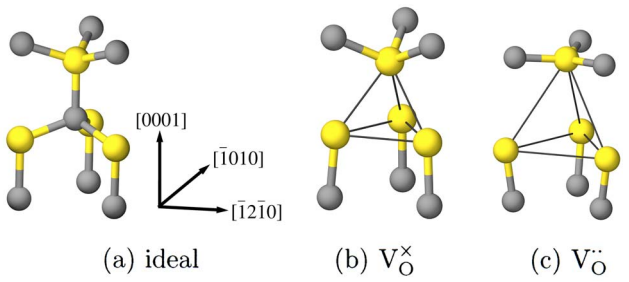

FIG. 2. (Color online) (a) Ideal wurtzite structure, (b) neutral oxygen vacancy, $V_O^{\times}$, and (c) charged oxygen vacancy, $V_O^{\cdot\cdot}$.

tion from the neutral state, $V_O^{\times}$, to the doubly positively charged state, $V_O^{\cdot\cdot}$, below the CBM.

For the neutral oxygen vacancy, $V_O^{\times}$, we observe an *inward* relaxation of the surrounding zinc atoms of approximately 11% (1.952 Å vs 1.733 Å) which form an almost perfect tetrahedron encapsulating the vacant site. On the other hand, a strong *outward* relaxation of about 19% is found for the charged vacancy, $V_O^{\cdot\cdot}$. Similar to the case of the neutral vacancy the atomic displacements are almost symmetric with respect to the vacant lattice site. Considering the configurations shown in Fig. 2 the strong upward movement of the central zinc atom is particularly noteworthy. In both cases, the first nearest neighbor shells exhibit significant relaxation, while the relaxation of second and farther neighbors is almost negligible. This observation is supported by the charge analysis, which shows that the cell charge is localized and practically exclusively accommodated by the nearest neighbor shell.

The doubly negative zinc vacancy, V''_{Zn}, is energetically favored under oxygen-rich conditions and for Fermi levels in the upper half of the band gap. In contrast to the oxygen vacancy, the geometric structure of the zinc vacancy is practically independent of the charge state. Our calculations show a symmetric outward relaxation of the first neighbor shell by about 14% while relaxations of farther neighbors are negligible.

2. Dumbbell interstitial

The geometric structure as well as the charge density of the neutral dumbbell interstitial, $O^{\times}_{i,db}$, [equivalent to $(O_2)^{\times}_O$, is shown in Fig. 3. The dumbbell interstitial, $O_{i,db}$, is characterized by two oxygen atoms which form a homo-nuclear bond and jointly occupy a regular oxygen lattice site. In addition, each of the two oxygen atoms forms two O—Zn bonds. The accumulation of charge along the O—O bond is indicative for a covalent bond. This oxygen interstitial defect conceptually resembles the well-known dumbbell interstitial defect in silicon (see, e.g., Ref. 22 and references therein) and some of its features remind of the nitrogen interstitial configuration in gallium nitride.[23]

The dumbbell geometry changes only marginally as the charge state varies between 2− and 2+. The bond lies in the ($\bar{1}2\bar{1}0$)-plane and is tilted with respect to the *c* axis by an angle between 45° and 51°. The presence of the defect causes outward displacements of the neighboring zinc atoms

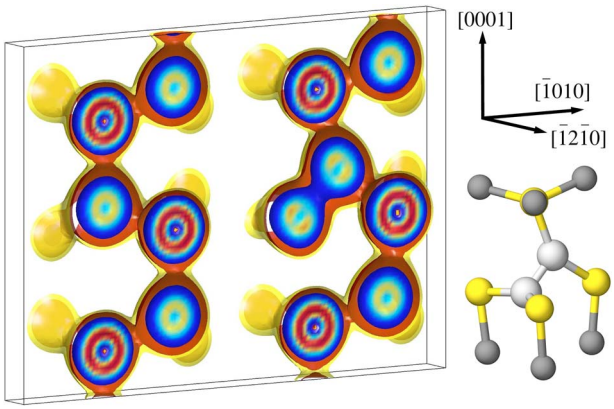

FIG. 3. (Color online) Geometry and electron density of dumbbell interstitial configuration, $O_{i,db}$. The electron density iso-surface plot shows a cut parallel to the ($\bar{1}2\bar{1}0$) plane. The illustration demonstrates the strong covalent bond between the two oxygen atoms of the dumbbell.

between −1.0% ($q=+2$) and −2.4% ($q=0$) if compared to the average nearest neighbor distance of the ideal structure. The largest relative displacement occurs for the uppermost zinc atom (~0.3 Å) which approaches the oxygen plane above. A similar displacement forces the lower oxygen atom of the dumbbell into the lower zinc plane. The separation of the two oxygen atoms, whose positions are nearly symmetric with respect to the ideal lattice site, varies between 1.423 Å ($q=+2$) and 1.485 Å ($q=-2$) which is 15% and 20% larger than the calculated bond length in the O_2 molecule (1.241 Å).

The electronic structure of this defect can be rationalized in terms of a simplified molecular orbital (MO) model (Fig. 4). The almost planar bonding configuration suggests the formation of sp^2-hybrid orbitals at both oxygen sites. Two out

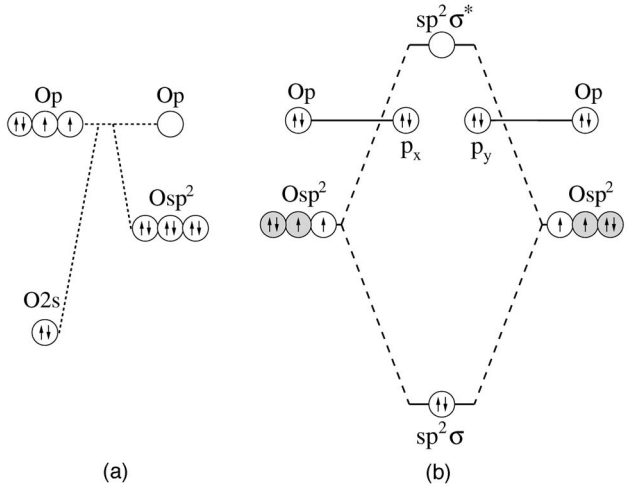

FIG. 4. (a) Formal hybridization of oxygen atoms prior to formation of the O-O bond. (b) Simplified MO scheme of the electronic structure of the oxygen dumbbell configuration in ZnO. The electron population corresponds to the neutral charge state. The orbitals shaded in gray and the electrons therein are being used for the formation of O-Zn bonds.

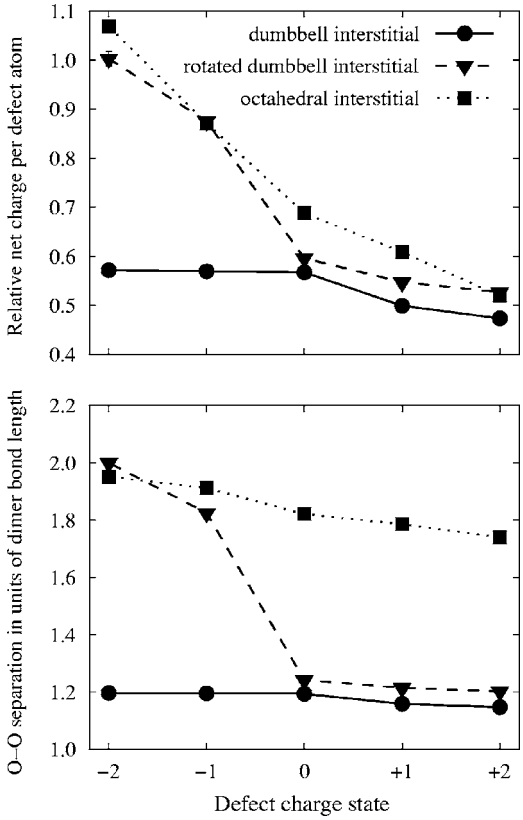

FIG. 5. Top: Relative net charge of oxygen atoms which are directly involved in interstitial configurations for different nominal charge states of the defect. Bottom: Variation of O-O bond distances as a function of the charge states of the defect. In the case of the octahedral interstitial, the O-O distances of the three nearest oxygen atoms of the second neighbor shell with respect to the central defect atom were evaluated.

of the three sp^2-orbitals at each oxygen site are involved in the formation of σ-bonds to the neighboring zinc atoms. Each oxygen atom contributes effectively 3/2 electrons to each of these bonds. The remaining singly occupied sp^2-hybrids form the O-O bond. The resulting bonding $sp^2\sigma$-orbital is fully occupied while the antibonding $sp^2\sigma^*$-orbital remains empty. The p-orbitals (one on each of the two atoms, labeled p_x and p_y in Fig. 4) are not hybridized and maintain an atomlike character, since they are orthogonal to each other [Figs. 3 and 6(b)]. In the case of the neutral dumbbell both of these (nonbonding) orbitals are fully occupied. In the following, the MO-scheme will turn out to be helpful for interpreting the geometric and electronic structure changes with charge state.

Figure 5 shows the result of the Bader analysis. Between the defect charge states 0 and 2+ the net charges decrease continuously. This corresponds to a continued oxidation of the two oxygen atoms starting from a formal oxidation number −I towards a formal oxidation number 0 although this limit is eventually not reached. Over the same range the formation energy stays practically constant (for a Fermi level close to the VBM, Table I) which according to the MO scheme occurs because the electrons in the unhybridized, atomlike p-orbitals can be removed at little energetic cost.

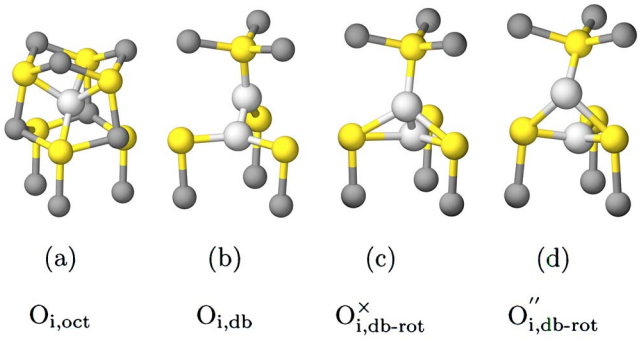

FIG. 6. (Color online) Overview of possible oxygen interstitial configurations. The yellow and dark gray spheres are the zinc and regular oxygen atoms, respectively. The interstitial oxygen atom(s) are colored in light gray. The (a) octahedral, $O_{i,oct}$, and (b) dumbbell, $O_{i,db}$, configurations are shown for the neutral charge state. In both cases the changes with varying charge state are continuous and rather small. In contrast, the rotated dumbbell interstitial displays a distinct geometry change as the charge state varies. The geometry which occurs for (c) the neutral charge state, $O^{\times}_{i,db\text{-}rot}$, is also representative for the positive charge states; on the other hand, (d) the doubly positive configuration, $O''_{i,db\text{-}rot}$, is prototypical for the negative charge states.

The slight decrease of the bond length can be related to a diminishing repulsion between the electron clouds localized on the atoms.

If the system is negatively charged in contrast the formation energy of the oxygen dumbbell increases significantly while the net charges remain constant. The negative surplus charge is smeared evenly over the cell. Compensation of the negative surplus charges by the oxygen–oxygen bond is impossible as it would imply population of the yet unoccupied antibonding σ^*-orbital and thus breakage of the bond. Since surplus electrons cannot be compensated in this geometry, the oxygen dumbbell interstitial, $O_{i,db}$, cannot act as an acceptor.

3. Rotated dumbbell interstitial

The geometry of the rotated dumbbell, $O_{i,db\text{-}rot}$, is shown for the neutral charge state in Fig. 6(c) and for the doubly negative charge state in Fig. 6(d). For the neutral and positive charge states the rotated dumbbell defect is characterized by a strong oxygen–oxygen bond akin to the regular dumbbell interstitial ($O_{i,db}$) discussed in the foregoing section. The bond is again confined to the $(\bar{1}2\bar{1}0)$-plane and tilted with respect to the c axis at an angle between 38° and 41° depending on charge state. In fact, the two dumbbell geometries are related to each other by a rotation of the oxygen bond about the $[10\bar{1}0]$ axis by an angle between $90°(q=+2)$ and $105°(q=0)$. The length of the oxygen–oxygen bond occurring for neutral and positive charge states is 20% to 24% larger than the bond length in the oxygen dimer and thus similar to the O-O separation in the regular dumbbell structure. In contrast to the dumbbell interstitial, however, each oxygen atom is bonded to three zinc atoms.

A very different behavior is found for the negative charge

states. The rotated dumbbell interstitial transforms into a *split-interstitial*. The two oxygen atoms maintain their mutually symmetric positions but are no longer bonded (Fig. 5) The split-interstitial configuration can therefore be regarded as two interstitial oxygen atoms associated with one oxygen vacancy.

Defect geometry and charge distribution underscore the similarity of the regular and rotated dumbbell in neutral and positive charge states (Fig. 5). As before, inspection of net charges reveals an almost perfect localization of the defect charge on both oxygen atoms forming the core of the defect. Going from charge state 1− to the neutral charge state the formation of the oxygen–oxygen bond is accompanied by a discontinuous decrease of the net charges by more than 30%.

For negative charge states, we observe that the surplus electrons are localized on the two oxygen atoms forming the split-configuration. This behavior is very distinct from the case of the dumbbell interstitial, $O_{i,db}$, for which delocalization of the extra charge is observed in the case of negatively charged cells. In fact, for the doubly negative charge state the defective oxygen atoms have achieved the same net charge state as oxygen atoms on a regular lattice and thus have a nominal oxidation number of −II. For these charge states, the rotated dumbbell interstitial, $O_{i,db\text{-}rot}$, strongly resembles the octahedral interstitial if net charge and O-O separation are considered as illustrated in Fig. 4. Unlike the case of the dumbbell interstitial, in both the octahedral as well as the rotated dumbbell configuration O—O bonds are absent. In summary, the oxygen atoms are able to adopt the formal oxidation state −II in the negative charge state limit and they approach the oxidation state 0 in the positive charge limit.

IV. DISCUSSION

The present calculations indicate that in neutral and positive charge states the energetically preferred mechanism for accomodation of surplus oxygen is the formation of an O—O bond. In such a configuration all bonds are saturated and electrons can be easily removed from nonbonding orbitals. Positive charge states of the dumbbell configurations have, therefore, low formation energies whence they can act as traps for holes in *p*-type doped samples. If the system is negatively charged, it strives to form additional (initially unsaturated) O—Zn bonds which are compensated by the surplus electrons. Therefore the split-interstitial and octahedral interstitial configurations are favorable for negative charge states.

In the regular dumbbell configuration, $O_{i,db}$, for negative charge states the two oxygen atoms are constrained to the dumbbell structure and are not able to break the O-O bond in order to adopt an energetically more favorable configuration. The opposite seems to apply for the positive charge states of the octahedral interstitial; the surplus oxygen atom strives to form oxygen–oxygen bonds, but it is encapsulated in a cage of zinc atoms, which it cannot leave without activation. Hence, in both cases energetic barriers exist, which give rise to large defect formation energies for the respective unfavorable charge states.

The rotated dumbbell interstitial, $O_{i,db\text{-}rot}$, incorporates the energetic advantage of oxygen–oxygen bonding for positive charge states, while for negative charge states the geometry allows breakage of the oxygen–oxygen bond and the formation of oxygen–zinc bonds. The resulting split-interstitial configuration for negative charge states involves the formation of four oxygen–zinc bonds for each atom of the oxygen pair. The defect energies reveal that the gain in energy due to the formation of three additional oxygen–zinc bonds by the two oxygen atoms in the split-interstitial configuration overcompensates the energetic cost for leaving the original oxygen site unoccupied as the formation energy of the rotated dumbbell interstitial is lower than the formation energy of the octahedral defect.

In summary, we have presented DFT calculations on stability and structure of oxygen interstitials and vacancies. The oxygen vacancy is the most stable defect for zinc-rich conditions. Under oxygen-rich conditions the zinc vacancy is energetically preferred for Fermi levels in the upper half of the band gap, while for Fermi levels in the lower half of the band gap oxygen interstitials in dumbbell configurations are the dominant defect types. These defects are characterized by a covalent oxygen–oxygen bond under neutral and positive charging. In the Introduction we have proposed a peroxolike defect and anticipated the possibility that the oxygen atoms forming the defect are oxidized as the Fermi level is pushed towards the VBM. The two dumbbell configurations, $O_{i,db}$ and $O_{i,db-rot}$, realize this proposition. In the neutral charge states the pair of oxygen atoms electronically resembles a single oxygen atom in an unperturbed crystal, nominally equivalent to $(O_2)_O^\times$. In this state both oxygen atoms are in the formal oxidation state −I. As the defect is charged increasingly positive the decreasing net charges of the atoms indicate further oxidation and the two dumbbell atoms approach a formal oxidation number of zero. The rotated dumbbell is a particular interesting case as the oxygen pair cannot only be oxidized (like the dumbbell interstitial), but is also able to assume a configuration in which the defect atoms carry a net charge equivalent to the ideal bulk value (oxidation state −II). This is achieved by breakage of the oxygen–oxygen bond in favor of the formation of several additional oxygen–zinc bonds. While the oxygen dumbbell configuration is a candidate for compensation of *p*-type doping under oxygen-rich conditions, the rotated dumbbell oxygen interstitial defect might also act as a compensating defect for *n*-type doping.

ACKNOWLEDGMENTS

We acknowledge generous grants of computer time by the Center for Scientific Computing at the Johann Wolfgang Goethe-University, Frankfurt/Main, and financial support through the *Sonderforschungsbereich 595* "Fatigue in functional materials" of the *Deutsche Forschungsgemeinschaft*.

[1] K. Ellmer, J. Phys. D **33**, R17 (2000).
[2] D. C. Look, B. Claflin, Y. I. Alivov, and S. J. Park, Phys. Status Solidi A **201**, 2203 (2004).
[3] C. G. Van de Walle, Physica B **308–310**, 899 (2001).
[4] S. B. Zhang, S.-H. Wei, and A. Zunger, J. Appl. Phys. **83**, 3192 (1998).
[5] H. Moormann, D. Kohl, and G. Heiland, Surf. Sci. **80**, 261 (1979).
[6] S. Trasatti, Electrochim. Acta **35**, 269 (1990).
[7] E.-C. Lee, Y.-S. Kim, Y.-G. Jin, and K. J. Chang, Phys. Rev. B **64**, 085120 (2001).
[8] S. B. Zhang, S. H. Wei, and A. Zunger, Phys. Rev. B **63**, 075205 (2001).
[9] A. F. Kohan, G. Ceder, D. Morgan, and Chris G. Van de Walle, Phys. Rev. B **61**, 15019 (2000).
[10] F. Oba, S. R. Nishitani, S. Isotani, H. Adachi, and I. Tanaka, J. Appl. Phys. **90**, 824 (2001).
[11] S. Limpijumnong, S. B. Zhang, S.-H. Wei, and C. H. Park, Phys. Rev. Lett. **92**, 155504 (2004).
[12] S. Goedecker, M. Teter, and J. Hutter, Phys. Rev. B **54**, 1703 (1996).
[13] X. Gonze, J.-M. Beuken, R. Caracas, F. Detraux, M. Fuchs, G.-M. Rignanese, L. Sindic, M. Verstraete, G. Zerah, F. Jollet, M. Torrent, A. Roy, M. Mikami, P. Ghosez, J. Y. Raty, and D. C. Allan, Comput. Mater. Sci. **25**, 478 (2002).
[14] The ABINIT code is a common project of the Université Catholique de Louvain, Corning Incorporated, and other contributors (URL http://www.abinit.org).
[15] S. Goedecker, SIAM J. Sci. Comput. (USA) **18**, 1605 (1997).
[16] M. C. Payne, M. P. Teter, D. C. Allan, T. A. Arias, and J. D. Joannopoulos, Rev. Mod. Phys. **64**, 1045 (1992).
[17] X. Gonze, Phys. Rev. B **54**, 4383 (1996).
[18] N. Troullier and J. L. Martins, Phys. Rev. B **43**, 1993 (1991).
[19] S. B. Zhang and J. E. Northrup, Phys. Rev. Lett. **67**, 2339 (1991).
[20] R. F. W. Bader, *Atoms in Molecules—A Quantum Theory* (Oxford University Press, Oxford, 1990).
[21] S. B. Zhang, S.-H. Wei, and A. Zunger, Phys. Rev. Lett. **84**, 1232 (2000).
[22] L. Colombo, Annu. Rev. Mater. Sci. **32**, 271 (2002).
[23] S. Limpijumnong and C. G. Van de Walle, Phys. Rev. B **69**, 035207 (2004).
[24] Zinc interstitials and antisite defects have been comprehensively described in literature earlier and are therefore not included in the present work.